

Statistical Dynamics of Spatial-order Formation by Communicating Cells

Eduardo P. Olimpio and Hyun Youk*

Kavli Institute of Nanoscience and

Departments of Bionanoscience and Physics, Delft University of Technology, 2629HZ Delft, The Netherlands

(Dated: May 25, 2022)

Communicating cells can coordinate their gene expressions to form spatial patterns. ‘Secrete-and-sense cells’ secrete and sense the same molecule to do so and are ubiquitous. Here we address why and how these cells, from disordered beginnings, can form spatial order through a statistical mechanics-type framework for cellular communication. Classifying cellular lattices by ‘macrostate’ variables - ‘spatial order parameter’ and average gene-expression level - reveals a conceptual picture: cellular lattices act as particles rolling down on ‘pseudo-energy landscapes’ shaped by a ‘Hamiltonian’ for cellular communication. Particles rolling down represent cells’ spatial order increasing. Particles trapped on the landscapes represent metastable spatial configurations. This framework is extendable to more complex forms of cellular communication.

Cells can communicate by secreting signaling molecules and this often underlies their collective behaviors. A striking example is initially uncoordinated cells, through cell-cell communication, coordinating their gene expressions to generate spatial patterns or structures [1–4]. Many cells partly or completely control such ‘disorder-to-order’ dynamics by simultaneously secreting and sensing the same signaling molecule [5, 6]. These ‘secrete-and-sense cells’ appear across diverse organisms and include quorum-sensing social amoeba *Dictyostelium* that form fruiting bodies [1, 2, 7] and autocrine-signaling T-cells [8, 9]. Based on mounting evidence from studies of different organisms [1–4, 6–8, 10–18], researchers now suspect that secrete-and-sense cells, many of which are governed by the same core genetic-circuit architecture [5, 19], are highly suited for spatially coordinating gene expressions. But if true, exactly why this is so, whether there are common design principles shared by different organisms, what the dynamics underlying their disorder-to-order transition is, and how to even quantify their spatial order, remain open questions. In this letter, we address these questions in the context of initially disordered fields of secrete-and-sense cells that self-organise into spatially ordered fields without any pre-existing morphogens. Specifically, we develop a theoretical framework that takes a simple and ubiquitous class of secrete-and-sense cells, sensibly defines and quantifies the notion of the cells’ spatial order, and then elucidates how the spatial order evolves over time using analytical methods. We focus here on analytically describing how spatial correlations among cells’ gene-expression levels dynamically emerge rather than on describing the shapes, sizes, and formations of specific spatial patterns (e.g., stripes). To study how specific patterns form, one often uses exhaustive numerical simulations that are adapted to particular organisms [20–23]. While such studies provide insights into spatial order formation, a theoretical framework may provide complementary insights that are difficult to extract from the often-large numbers of parameters

involved in numerical simulations. But a suitable theoretical framework for secrete-and-sense cells is currently lacking.

Our main idea is that describing hundreds of secrete-and-sense cells forming a particular spatial configuration is infeasible without exhaustive numerical simulations but that it is possible to analytically describe how an ensemble of ‘similar’ spatial configurations evolves over time without knowing the state of each cell. We will define a ‘spatial order parameter’ - a number between zero (complete disorder) and one (complete order). Inspired by statistical physics-approaches, we will group all lattices of cells that have the same spatial order parameter and average gene-expression level into an ensemble (‘macrostate’). Surprisingly, we find that this macrostate moves like a particle that drifts-and-diffuses in an abstract space (‘phase space’) whose coordinates denote the cells’ spatial order and average gene-expression level. The particle drifts down a ‘pseudo-energy landscape’ defined by a ‘Hamiltonian’ for cell-cell communication that is akin to Hamiltonians of frustrated magnets. We thus provide an intuitive picture, based on measurable quantities, that is both practical and conceptual for elucidating how cells spatially coordinate their gene expressions.

We used a cellular automaton [24] to simulate secrete-and-sense cells. We will compare its results with our theory. We considered a two-dimensional triangular lattice of N spherical, immobile secrete-and-sense cells of radius R and lattice spacing a_0 . As a proof-of-principle, we considered ‘simple’ secrete-and-sense cells that (1) very slowly respond to their fast diffusing signal, and (2) whose ‘output-gene’ expression level, which is determined by the extracellular concentration of the signal, and signal-secretion rate exhibit switch-like (digital) bistability [19]. These two features were motivated by experimentally characterised secrete-and-sense cells. Examples include yeasts that secrete-and-sense a mating pheromone in a nearly digital manner (diffusion timescale ~ 1 s; response timescale ~ 30 minutes)[6, 25]

and mouse hair follicles, which are secrete-and-sense organs that act as digital secrete-and-sense cells on a triangular lattice (diffusion timescale ~ 12 hours; response timescale ~ 1.5 days)[23]. Each cell's output-gene expression is either 'ON' (and its signal-secretion rate is 'high') or 'OFF' (and its signal-secretion rate is 'low'). Each cell senses the steady-state signal-concentration c on itself. If c is larger (lower) than a threshold concentration K , then the cell is ON (OFF). When $N = 1$, an ON-cell (OFF-cell) maintains a steady-state concentration C_{ON} (C_{OFF}) on itself. We set $C_{OFF}=1$. The cellular automaton computes the c on every cell, synchronously updates each cell's state, and repeats this process until it reaches a steady-state in which no cell requires an update. By running the cellular automaton on randomly distributed ON- and OFF-cells, we observed that initially disordered lattices could indeed evolve into spatially ordered steady-state configurations such as islands of ON-cells (Fig. 1a)[26].

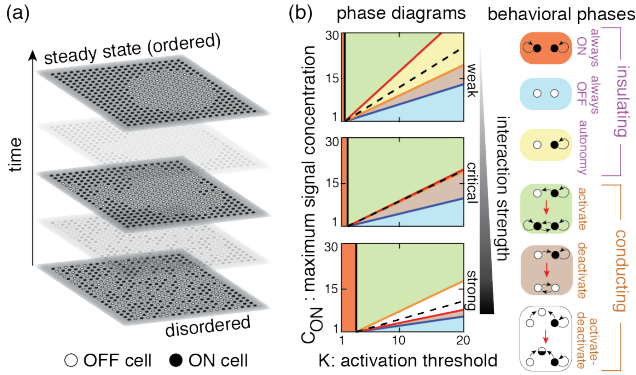


Figure 1. Behavioral phases of secrete-and-sense cells. (a) Snapshots of disorder-to-order transition dynamics. (b) (Left column): Phase diagrams for weak interaction (top), critical interaction (middle), and strong interaction (bottom). (Right column): Distinct behavioral phases in different colors.

To reveal how the disorder-to-order dynamics arises, we will analyse the cellular automaton in each of the cells' 'behavioral phases' that we described in a previous work (Fig. 1b) [19, 26]. To recap, the behavioral phases represent how one cell turns on/off another cell. They arise from self-communication (i.e., a cell captures its own signal) competing with neighbor-communication (i.e., a cell captures the other cells' signal). This competition is characterised by an 'interaction strength', $f_N(a_o) \equiv \sum_{i,j} e^{R-r_{ij}}/r_{ij}$ (where r_{ij} is the distance between cell i and cell j in units of a_o). It measures how much of the other cells' signal diffuses to each cell [19, 26]. Given an interaction strength, the K and C_{ON} determine the cells' behavioral phase. The values of K , C_{ON} , and $f_N(a_o)$ are held fixed and thus the cells' behavioral phase also remains unchanged over time. A behavioral phase is either an 'insulating phase' - in which no cell can turn on/off the other cells due to dominant self-

communication - or a 'conducting phase' - in which cells can turn on/off the others due to dominant neighbor-communication (Fig. 1b). Regardless of the interaction strength, cells can operate in two conducting phases: (1) 'activate phase' - in which nearest neighbor ON-cells can turn on an OFF-cell, and (2) 'deactivate phase' - in which nearest neighbor OFF-cells can turn off an ON-cell. Additionally, when the interaction is weak (i.e., $f_N(a_o) < 1$), cells can operate in 'autonomy phase' - an insulating phase in which a cell can stay ON/OFF regardless of the other cells' states. On the other hand, when the interaction is strong (i.e., $f_N(a_o) > 1$), cells can operate in 'activate-deactivate phase' - a conducting phase in which the cells can both activate and deactivate others depending on their relative locations [19].

We now present our theory's central ingredient. Let us define two 'macrostate' variables: (1) the fraction p of cells that are ON (equivalent to the average output-gene expression level) and (2) a 'spatial order parameter' I defined as

$$I \equiv \frac{N}{\sum_{i,j} f(r_{ij})} \frac{\sum_{i,j} f(r_{ij}) (X_i - \langle X \rangle) (X_j - \langle X \rangle)}{\sum_i (X_i - \langle X \rangle)^2} \quad (1)$$

where $f(r_{ij}) \equiv e^{R-r_{ij}}/r_{ij}$ is the cell-pair- ij 's interaction term, and X_i is $+1$ (-1) for an ON (OFF)-cell. By definition, $0 \leq |I| \leq 1$ and $0 \leq p \leq 1$. Roughly speaking, the I measures the average correlation between any two cells by weighing each cell pair by its interaction strength [19, 26, 27]. As $|I|$ approaches 0, the lattice becomes more disordered. As $|I|$ approaches 1, the lattice becomes more ordered. When $I = 0$, ON- and OFF-cells are randomly distributed, yielding maximally disordered lattices. Our central idea is to group cellular lattices that have the same (p, I) into an ensemble (i.e., macrostate) (examples in Fig. 2a and [19]). We then view a macrostate as a particle that moves in an abstract space (i.e., 'phase space') whose position at time t is $(p(t), I(t))$. Each point (p, I) in this phase space represents an ensemble of thousands of spatial configurations ('microstates') [19]. By randomly choosing thousands of microstates that all belong to the same disordered macrostate ($p_{\text{initial}}, 0$) and then running the cellular automaton on each one, we observed how the lattices evolved out of disorder (Fig. 2b). Specifically, we obtained a distribution of their trajectories (thus also a distribution of their final positions ($p_{\text{final}}, I_{\text{final}}$)) for each value of p_{initial} in each behavioral phase (Fig. 2b) [19]. The fact that we obtained distributions of trajectories for each p_{initial} , instead of a single trajectory, highlights that the particle moves stochastically. This arises from the automaton operating on individual cell's state X_i - a microstate variable that we ignore - rather than on the macrostate variables, p and I . We observed that in every trajectory, the I initially increased before plateauing while the p either increased or decreased over time (Fig. 2b). Then, one of two events occurred: either (1) the particle stopped before its p reached an extreme value

(i.e., zero or one) (e.g., green trajectories in the activate-deactivate phase in Fig. 2b); or (2) the particle reached an extreme value of p and as it did so, its I abruptly dropped to zero (e.g., red trajectories in Fig. 2b).

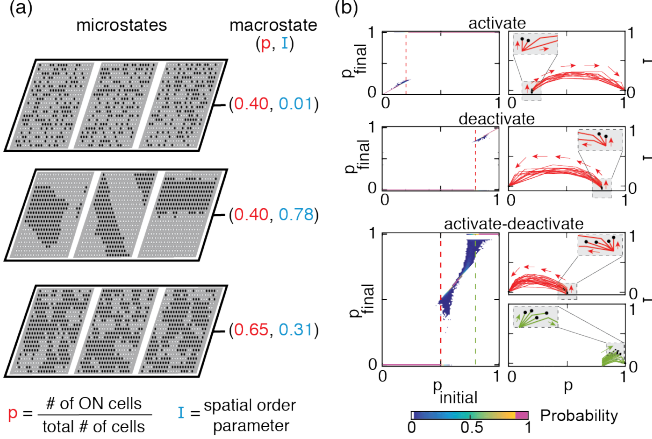


Figure 2. Macrostates of secrete-and-sense cells. (a) Examples of microstates grouped into a macrostate. p = average output-gene expression level (equivalent to fraction of cells that are ON), I = spatial order parameter. (p, I) defines a macrostate. (b) (left column) Probability density maps of the particle's final value of p (denoted p_{final}) for every initial value of p (denoted p_{initial}). (right column) Trajectories (red and green curves) in p - I space in the activate phase (top), deactivate phase (middle), and activate-deactivate phase (bottom). Grey insets show zoomed-in views of trajectories. Black dots denote trajectories' endpoints.

We sought the particle's equation of motion that recapitulates these features. We first rewrite Eq. (1) as

$$I = \frac{\Theta - (2p - 1)^2 f_N(a_o)}{4p(1 - p)f_N(a_o)}, \quad (2)$$

where we have defined a 'normalized spatial order', $\Theta \equiv \langle \sum_{i,j} f(r_{ij}) X_i X_j \rangle$. The Θ and thus the $|I|$ are bounded above for each value of p since there is a finite number of ways to arrange the fixed number of ON-cells. Specifically, as p nears zero or one, Eq. (2) shows that the maximally allowed I sharply decreases to zero (see black curves in Fig. 3) [19]. This explains why the particle's I abruptly drops to zero as its p reaches zero or one (Fig. 2b). Yet, here the cells are becoming more correlated since every cell is either turning on ($p=1$) or off ($p=0$). Thus, we must interpret the I carefully near the extreme values of p . Conveniently, the Θ , which also measures the average correlation between two cells by weighing their interaction strength, always increases as the cells become more correlated. Thus, we sought equations of motion in terms of p and Θ . We conjectured that the particles follow a Langevin-type dynamics:

$$p(t+1) = p(t) + \langle \Delta p(t) \rangle + \eta_{\Delta p}(t) \quad (3a)$$

$$\Theta(t+1) = \Theta(t) + \langle \Delta \Theta(t) \rangle + \eta_{\Delta \Theta}(t), \quad (3b)$$

where $\Delta p(t)$ and $\Delta \Theta(t)$ are changes in p and Θ respectively between t and $t+1$, and $\eta_{\Delta p}$ and $\eta_{\Delta \Theta}$ are noise terms that represent our ignorance of the microstates. From calculating the probability of an ON (OFF)-cell turning off (on) after one time step as a function of p , we could estimate $\langle \Delta p(t) \rangle$, $\langle \Delta \Theta(t) \rangle$, and variances of $\eta_{\Delta p}(t)$ and $\eta_{\Delta \Theta}(t)$ [19]. Then, by running Monte Carlo simulations that obey these statistics [19], we obtained particle trajectories dictated by Eq. (3) and compared them to those produced by the cellular automaton. From this, we found that Eq. (3) misses several aspects but recapitulates the main features, including where the particles stop (e.g., distributions shown in Fig. 3a) and the average number of time steps required to form steady-state configurations (Fig. 3b).

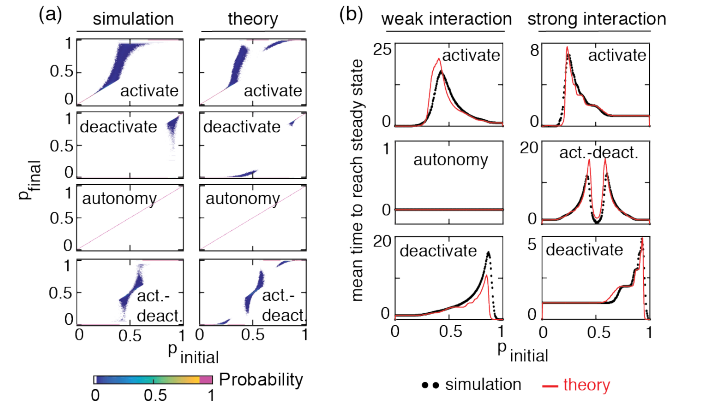


Figure 3. Comparison between simulations and theory. (a) Probability density maps of p_{final} (final value of p) for every p_{initial} (initial value of p) produced by the cellular automaton (left column) and our theory (from Eq. (3)) (right column). (b) Average time that cells take to generate steady-state configurations as a function of p_{initial} , estimated by our theory (red curves, based on Eq. (3)) and by the cellular automaton (black points) for a weak interaction (left column) and a strong interaction (right column).

Ignoring the microstates causes the diffusion. But what causes the particle to drift so that the cells gradually become more spatially ordered? If the particle picture is truly valid, then there may be a landscape on which the particles roll down and this may explain the drift. To explore this idea, we define a 'multicellular Hamiltonian', $h \equiv -\sum_i X_i (Y_i - K)/N$, where Y_i is the signal concentration on cell- i . In fact, we can rewrite h entirely in terms of the macrostate variables, p and I [19]. Plotting $h(p, I)$ yields a 'pseudo-energy landscape' (Fig. 4a). Its shape depends on the cells' behavioral phase (Figs. 4b-4d). Importantly, by plotting the trajectories on top of their respective landscapes, we observed that every particle's pseudo-energy monotonically decreased over time until the particle stopped - a fact that we could also rigorously prove [19]. Crucially, in every behavioral phase, the pseudo-energy land-

scape slopes downwards towards increasing I (Figs. 4b–4d). Moreover, the position of the pseudo-energy landscape’s peak, which occurs at $I \approx 0$ in every behavioral phase (Figs. 4b–4d), determines whether the particle subsequently rolls down towards increasing or decreasing p . The particles cannot roll all the way down because for each value of p , there is a maximally allowed value of I (black curves in Figs. 4b–4d), which we can estimate [19]. To see at the microstate-level why the cells become more spatially correlated over time, we rewrite the h as

$$h = -\alpha \sum_{i,j} f(r_{ij}) X_i X_j - B \sum_i X_i - N\alpha, \quad (4)$$

where $\alpha \equiv (C_{ON} - 1)/(2N)$, and B is a ‘signal field’ identified as $\alpha(1 + f_N(a_o)) - K/N$. Eq. 4 is strikingly similar to the Hamiltonians of Hopfield network [28] and magnetic spins with long-range interactions [29]. As in physical systems, the signal field is a knob that an experimentalist (and cells) can tune to sculpt the pseudo-energy landscape [19]. It competes with the cell-cell interaction term in Eq. (4) (with coupling constant $\alpha f(r_{ij})$). From the phase diagrams, we can deduce that $B > 0$ in the activate phase, that $B < 0$ in the deactivate phase, and that B can be positive, negative, and zero in the activate-deactivate phase (depending on K and C_{ON}) [19]. Intuitively, increasing the Θ corresponds to more clusters of ON-cells and OFF-cells forming, which would in turn decrease the Hamiltonian since averaging the first term in Eq. 4 yields $-\alpha\Theta$. As seen here, the pseudo-energy landscape provides an intuitive picture, at the microstate- and macrostate-levels, of how and why the cells become more ordered over time.

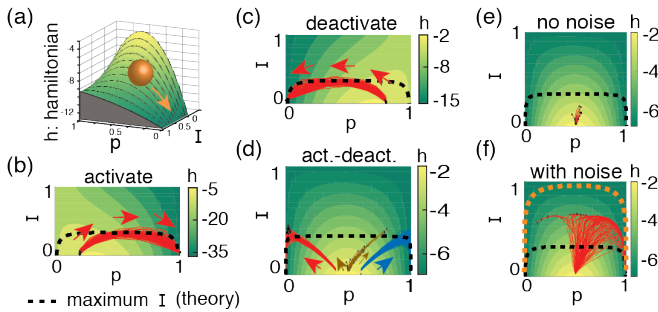


Figure 4. Cellular lattices act as particles drifting-and-diffusing downwards on pseudo-energy landscapes. (a) Pseudo-energy landscape defined by Hamiltonian $h(p, I)$ for cellular communication. Pseudo-energy landscape for (b) activate phase, (c) deactivate phase, and (d-f) activate-deactivate phase. (b-f) Trajectories of the same color start from the same position in each landscape. Black curves show maximally allowed I [19]. Trajectories without noise (e) and with noise (f) on the same landscape. Orange curve in (f) is maximally allowed I when moderate noise is present [19].

Unlike physical energy landscapes, however, the pseudo-energy landscape can trap particles at its sloped

regions, particularly but not exclusively in the activate-deactivate phase. We see this in the brown trajectories in Fig. 4d and the red trajectories in Fig. 4e. These trajectories all terminate at intermediate values of p , before reaching the absolute minima of h . These trapped particles represent steady-state spatial configurations. At the macrostate-level, the trappings arise because p and I must change together due to I ’s dependence on p . Thus many regions of the pseudo-energy landscape are inaccessible (e.g., the bound on I placed by the black ‘fence’ in Figs. 4b–4e). At the microstate-level, the trappings arise due to a geometric restriction that is similar in flavor to, but not the same as, the geometric frustrations in magnetic spins [30]. For example, in certain regions of the activate-deactivate phase, if we consider a lattice consisting of just five ON-cells in a cluster, we can show that for an OFF-cell to turn on, at least three of its nearest neighbours must be on whereas for an ON-cell to turn off, at least five of its nearest neighbours must be on [19]. Since the lattice is triangular, neither of the two conditions can be met even though both would decrease the pseudo-energy. Hence the particle that represents this lattice would be trapped.

Finally, as a proof-or-principle for showing how to include stochastic gene expressions [31–36], we added stochastic sensing to the cellular automaton. We allowed the K to fluctuate around a mean K_o with a standard deviation δK , from cell to cell and from time to time. We found that noise could liberate trapped particles [19]. In this sense, the trapped particles represent metastable spatial configurations. In particular, we found that a moderate noise, which occurs when $\delta K \sim \min(|\langle Y_{ON} \rangle - K_o|, |\langle Y_{OFF} \rangle - K_o|)$ (where $\langle Y_{ON(OFF)} \rangle$ is the mean signal-concentration on an ON (OFF)-cell), could liberate trapped particles and push them further down the landscape, beyond the previously allowed region, until they became trapped in regions of higher spatial order (compare Fig. 4f with Fig. 4e). These particles also cannot roll to the bottom because, just as when the sensing was deterministic, we found that a maximally allowed value of I exists for every p when a moderate noise is present (orange curve in Fig. 4f) [19]. Intriguingly, we observed that some of these newly trapped particles’ p , I , and h changed very slowly, allowing them to remain trapped at an intermediate p over hundreds but not thousands of time steps [19]. We expect a follow-up study to examine if this is related to glass-type dynamics.

Here we uncovered a visual landscape for cellular communication and showed that it underlies why and how simple secrete-and-sense cells’ gene expressions become more spatially correlated over time. In the process, we revealed connections between secrete-and-sense cells, drifting-and-diffusing particles, and magnetic spins by defining quantities whose names originate from statistical mechanics but whose meanings are adapted to describe gene expressions of communicating cells. The theory does

not yet account for more complex forms of secrete-and-sense cells. But it opens up a possibility of analytically studying them since they share the same basic genetic-circuit architecture (albeit with added complexity) [5] as the one studied here. Considering other forms of cellular communication may also be fruitful. Towards this end, we show in the Supplementary Material [19] how to extend our framework to lattices with multiple cell-types and signal-types, including paracrine-signaling [5, 37]. Our work and its extensions may help guide experiments as well since p and I are measurable, for example, in microscope-based time-lapse movies of cells expressing fluorescent proteins. We hope that our work, along with complementary approaches for studying spatial patterns [20, 21, 38–43], will inform on-going efforts to establish generic frameworks for multicellular gene regulations.

We thank Pieter Rein ten Wolde, Arjun Raj, Louis Reese, and Yaroslav Blanter for insightful discussions. HY was supported by the European Research Council and the Dutch Organization for Scientific Research.

* h.youk@tudelft.nl

- [1] T. Gregor, K. Fujimoto, N. Masaki, and S. Sawai, *Science* **328**, 1021 (2010).
- [2] S. Sawai, P. A. Thomason, and E. C. Cox, *Nature* **433**, 323 (2005).
- [3] T. Danino, O. Mondragón-Palomino, L. Tsimring, and J. Hasty, *Nature* **463**, 326 (2010).
- [4] C. Liu, X. Fu, L. Liu, X. Ren, C. K. L. Chau, S. Li, L. Xiang, H. Zeng, G. Chen, L.-H. Tang, P. Lenz, X. Cui, W. Huang, T. Hwa, and J.-D. Huang, *Science* **334**, 238 (2011).
- [5] B. A. Doğaner, L. K. Q. Yan, and H. Youk, *Trends Cell Biol.* **26**, 262 (2016).
- [6] H. Youk and W. A. Lim, *Science* **343**, 1242782 (2014).
- [7] A. E. Sgro, D. J. Schwab, J. Noorbakhsh, T. Mestler, P. Mehta, and T. Gregor, *Mol. Syst. Biol.* **11**, 779 (2015).
- [8] Y. E. Antebi, S. Reich-Zeliger, Y. Hart, A. Mayo, I. Eizenberg, J. Rimer, P. Putheti, D. Pe’er, and N. Friedman, *PLoS Biol.* **11**, e1001616 (2013).
- [9] M. B. Sporn and G. J. Todaro, *N. Engl. J. Med.* **303**, 878 (1980).
- [10] P. Mehta, S. Goyal, T. Long, B. L. Bassler, and N. S. Wingreen, *Mol. Syst. Biol.* **5**, 1 (2009).
- [11] K. Kamino, Y. Kondo, A. Nakajima, M. Honda-Kitahara, K. Kaneko, and S. Sawai, *Proc. Natl. Acad. Sci. U.S.A.* **114**, E4149 (2017).
- [12] Y. Hart, S. Reich-Zeliger, Y. E. Antebi, I. Zaretsky, A. E. Mayo, U. Alon, and N. Friedman, *Cell* **158**, 1022 (2014).
- [13] S. De Monte, F. d’Ovidio, S. Danø, and P. G. Sørensen, *Proc. Natl. Acad. Sci. U.S.A.* **104**, 18377 (2007).
- [14] T. Umeda and K. Inouye, *J. Theor. Biol.* **226**, 215 (2004).
- [15] L. You, R. S. Cox, R. Weiss, and F. H. Arnold, *Nature* **428**, 868 (2004).
- [16] A. Pai, Y. Tanouchi, and L. You, *Proc. Natl. Acad. Sci. U.S.A.* **109**, 19810 (2012).
- [17] M. Coppey, A. M. Berezhkovskii, S. C. Sealton, and S. Y. Shvartsman, *Biophys. J.* **93**, 1917 (2007).
- [18] S. Y. Shvartsman, H. S. Wiley, and W. M. Deen, *Biophys. J.* **81**, 1854 (2001).
- [19] See Supplementary Material for step-by-step derivations, supplementary figures, and additional discussions.
- [20] J. Cotterell and J. Sharpe, *Mol. Syst. Biol.* **6**, 1 (2010).
- [21] J. Cotterell, A. Robert-Moreno, and J. Sharpe, *Cell Syst.* **1**, 257 (2015).
- [22] M. Haskel-Ittah, D. Ben-Zvi, D. Branski-Arieli, E. D. Schejter, B.-Z. Shilo, and N. Barkai, *Cell* **150**, 1016 (2012).
- [23] C.-C. Chen, L. Wang, M. V. Plikus, T. X. Jiang, P. J. Murray, R. Ramos, C. F. Guerrero-Juarez, M. W. Hughes, O. K. Lee, S. Shi, R. B. Widelitz, A. D. Lander, and C. M. Chuong, *Cell* **161**, 277 (2015).
- [24] G. B. Ermentrout and L. Edelstein-Keshet, *J. Theor. Biol.* **160**, 97 (1993).
- [25] N. Rappaport and N. Barkai, *J. Biol. Phys.* **38**, 267 (2012).
- [26] T. Maire and H. Youk, *Cell Syst.* **1**, 349 (2015).
- [27] P. A. P. MORAN, *Biometrika* **37**, 17 (1950).
- [28] J. J. Hopfield, *Proc. Natl. Acad. Sci. U.S.A.* **79**, 2554 (1982).
- [29] S. Kirkpatrick and D. Sherrington, *Phys. Rev. Lett.* **35**, 1792 (1975).
- [30] O. Tchernyshyov and G.-W. Chern, *Spin-lattice coupling in frustrated antiferromagnets* (Springer, 2011).
- [31] F. Sagués, J. M. Sancho, and J. García-Ojalvo, *Rev. Mod. Phys.* **79**, 829 (2007).
- [32] J. García-Ojalvo, *Contemporary Physics* **52**, 439 (2011).
- [33] G. Tkačik and A. M. Walczak, *J. Phys. Condens. Matter* **23**, 153102 (2011).
- [34] A. Sanchez and I. Golding, *Science* **342**, 1188 (2013).
- [35] H. Xu, S. O. Skinner, A. M. Sokac, and I. Golding, *Phys. Rev. Lett.* **117** (2016).
- [36] N. Friedman, L. Cai, and X. S. Xie, *Phys. Rev. Lett.* **97** (2006).
- [37] In paracrine signaling, one cell secretes a signal without sensing it while another cell senses without secreting that signal.
- [38] S. Surkova, A. V. Spirov, and V. V. Gursky, *PLoS Comp. Biol.* **5**, e1000303 (2009).
- [39] T. R. Sokolowski, T. Erdmann, and P. R. ten Wolde, *PLoS Comp. Biol.* **8**, e1002654 (2012).
- [40] G. Tkačik, T. Gregor, and W. Bialek, *PLoS ONE* **3**, e2774 (2008).
- [41] P. Hillenbrand, U. Gerland, and G. Tkačik, *PLoS ONE* **11**, e0163628 (2016).
- [42] T. Erdmann, M. Howard, and P. R. ten Wolde, *Phys. Rev. Lett.* **103**, 258101 (2009).
- [43] S. Fancher and A. Mugler, *Phys. Rev. Lett.* **118**, 078101 (2017).